The induction zone/factor and sheared inflow: A linear connection?

Meyer Forsting, AR; van der Laan, MP; Troldborg, Niels

Published in:
Journal of Physics: Conference Series

Link to article, DOI:
10.1088/1742-6596/1037/7/072031

Publication date:
2018

Document Version
Publisher's PDF, also known as Version of record

The induction zone/factor and sheared inflow: A linear connection?

IOP Conf. Series: Journal of Physics: Conf. Series **1037** (2018) 072031 doi:10.1088/1742-6596/1037/7/072031

The induction zone/factor and sheared inflow: A linear connection?

AR Meyer Forsting[1], MP van der Laan[1], N Troldborg[1]

[1] DTU Wind Energy, Technical University of Denmark, Risø Campus, DK-4000 Roskilde, Denmark

E-mail: alrf@dtu.dk

Abstract. Sheared inflow causes significant periodic load variations in wind turbine blades, but has only limited impact on the mean wake deficit. Following these findings the wind speed reduction upstream of the turbine - referred to as the induction zone - might also show little difference to uniform inflow. Using the local free-stream velocity to normalise the upstream flow-field should then render uniform and sheared inflow induced velocity profiles indiscernible, hinting towards wind shear acting solely as a linear addition. This has great implications in BEM methods for determining the velocity at the blades and also for near-rotor lidar measurements. The latter being applied in for power/loads assessment and turbine control. LES simulations with an actuator line representation of the rotor confirm the linearity assumption for moderate wind shear. To estimate the normal velocities at the disc the annularly averaged thrust coefficient is best suited, when the induction is imposed on the inflow profile. A strictly local relationship breaks down in strongly sheared flow. A simple induction zone model devised for uniform inflow estimates the velocity upstream within $\pm 0.5\%$ even at extreme shear in the upper half of the rotor and at least three rotor radii away from the turbine.

1. Introduction

The flow incoming towards a wind turbine rotor is continuously decelerated by the rotor's thrust force acting on it. The thrust is in turn a result of the aerodynamic forces acting over the rotor blades, which are directly linked to the velocities normal to the rotor plane. The free-stream or inflow velocity, V_∞, is related to the normal/axial velocity, u, through the induction factor a, such that $u = V_\infty(1-a)$. This factor essentially quantifies the deceleration introduced by the rotor forces. In sheared inflow V_∞ becomes a function of height z, but what about a? Field measurements and simulations by Meyer Forsting *et al.* [1] - supported by Simley *et al.* [2] - show a near constant a with height, when computed locally i.e. $a_{\text{shear}}(\mathbf{x}) = 1 - u(\mathbf{x})/V_\infty(z) = a_{\text{uniform}}(\mathbf{x})$. In fact following this normalisation little difference in the flow-field upstream is found between uniform and moderately sheared inflow. This suggests that shear solely acts as linear perturbation to the the rotor flow for moderate shear. This has great implications for near-rotor lidar measurements, from which the free-stream velocity is estimated as reference for power and loads assessments. An induction zone model for uniform inflow [3] could thus be applied to sheared inflow, when assuming a certain velocity profile [4]. Despite first signs for an equivalence between uniform and sheared inflow a more thorough and quantitative analysis is needed with respect to eventual non-linear effects at high thrust and extreme levels of shear. Previously the rotor was represented by constantly loaded discs,

whereas in this study individual blades and their corresponding aerodynamic data are included.

2. Computational method

2.1. Flow solver and modelling approach

The finite-volume solver, EllipSys3D, discretises the Navier-Stokes equations over a block-structured domain [5]. The turbulence is either modelled by a Reynolds-averaged Navier-Stokes (RANS) formulation with a Menter $k-\omega$ shear-stress transport (SST) closure [6] or by solving the filtered Navier-Stokes equations with a sub-grid scale (SGS) model. Switching between models is determined by a limiter function as defined by Strelets [8]. This also determines whether the QUICK [9] (RANS) or a fourth-order CDS scheme (LES) discretises the convective terms. The shear is specified at the inflow boundary in form of a power law $V_\infty(z) = V_{\infty,\mathrm{hub}} \left(\frac{z+z_\mathrm{hub}}{z_\mathrm{hub}}\right)^\alpha$. The rotor forces of the NREL 5-MW [10] with a hub height of 90 m and 63 m blades are introduced by an actuator line (AL) [11].

2.2. Numerical setup

The numerical domain is defined as in preceding studies and detailed in [1]. The grid spacing around the rotor is $R/32$, where R represents the rotor radius.

The atmospheric boundary layer is assumed to follow a power law with $\alpha = \{0, 0.1, 0.3, 0.5\}$. As the blade forces are directly linked to the available kinetic energy sampled by the turbine $F \int_A \frac{1}{2}\rho V_\infty^2(\mathbf{x})\,\mathrm{d}A$ it is kept constant for the different shear profiles. The rotor-based Reynolds number is kept far above 10^5 [12] and the time step is set to 0.03 s at 9.2 rotations per minute. The smearing factor is set to twice the grid spacing and the tip correction by Shen *et al.* [13] is used with a modified constant $c_2 = 33$. The latter are chosen to fit the results of the full rotor simulations presented in [14].

3. Results and Discussion

All following results and analyses are based on time-averaged quantities. The averaging period encompasses 10 minutes, converging the residual of the mean quantities to 10^{-5}.

3.1. Thrust and induced velocities at the disc

The influence of strong shear ($\alpha = 0.5$) on the time-averaged normal velocities at the rotor disc is shown in figure 1. Following the inflow profile the velocities increase with distance from the ground. However, the disc velocities do not only depend on z, but also exhibit an annular correlation. Without shear ($\alpha = 0$) all velocity variation over the disc occurs in the radial direction - in line with the blade forces. If shear acts as a linear perturbation to the induced velocities, the local induction factors, $a(\mathbf{x})$, should be independent of the shear i.e. by normalising with the respective inflow profile, $V_\infty(\mathbf{x})$, the effect of shear should vanish. This assumption holds for moderate shear ($\alpha = 0.1$), but not for more extreme scenarios as shown in figure 2 where $\alpha = 0.5$. Relative to the mean induction, there is a substantial increase of up to 60% in the induction on the blades close to the ground. On the upper half of disc, on the other hand, the induction is close to the mean. As for the normal velocity a clear annular correlation persists in the disc induction. The strong induction close to the ground hints towards equally elevated blade forces. A measure of the local forcing is given by the local thrust coefficient, which is defined as:

$$C_t(\mathbf{x}) = \frac{f_N(\mathbf{x})}{1/2\rho V_\infty^2(\mathbf{x})} \tag{1}$$

Here f_N represents the normal force and ρ air density. Figure 3 shows the variation in the local thrust coefficient over the disc for the same flow as in figures 1 and 2. The pattern here is similar to the induction, yet the variations are much stronger with a peak increase beyond 100%.

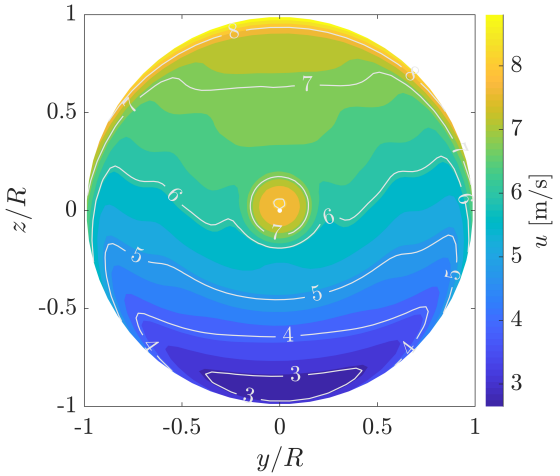

Figure 1. Time-averaged normal/axial velocity at the rotor disc for $\alpha = 0.5$. (LES simulation)

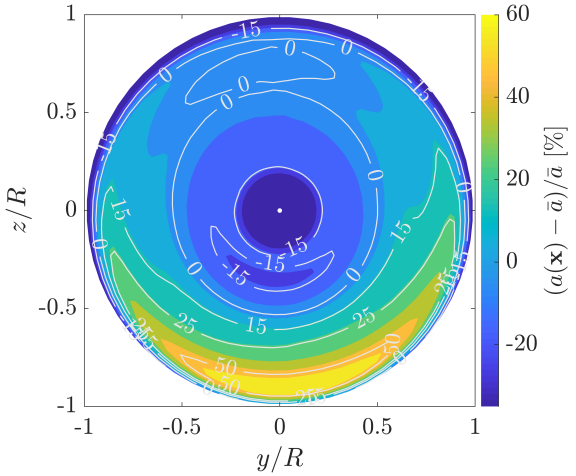

Figure 2. Time-averaged locally induction factor relative to rotor disc average ($\bar{a} = 0.270$) for $\alpha = 0.5$ at the turbine. Here $a(\mathbf{x}) = 1 - u(\mathbf{x})/V_\infty(\mathbf{x})$. (LES simulation)

Figure 4 portrays the breakdown of classic momentum theory between strictly local thrust and induction (figures 2 and 3). The simulation results are represented in form of an intensity map and compared to the Blade Element Momentum (BEM) prediction as well as the polynomial fit suggested by Madsen [15] (similar to Glauert's fit) for large thrust coefficients. The highest intensity is seen close to the theoretical prediction, resulting in the disc averaged thrust and induction to fully agree with theory. Yet a large fraction of the LES results show extreme local thrust values with respect to the induced velocity. With decreasing shear the deviation also

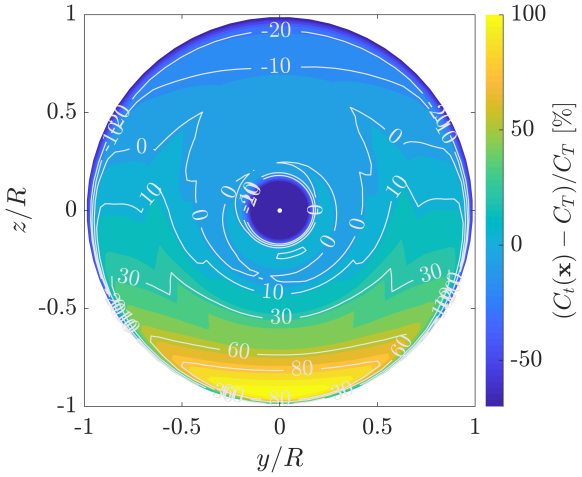

Figure 3. Local relative to global thrust coefficient ($C_T = 0.797$) for $\alpha = 0.5$. (LES simulation)

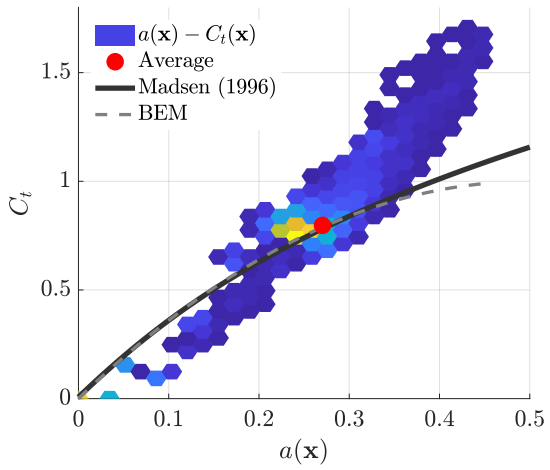

Figure 4. Intensity map of the local thrust, $C_t(\mathbf{x})$, versus local induction, $a(\mathbf{x})$, derived from the LES simulations for $\alpha = 0.5$ compared to theoretical and empirical relations.

diminishes and nearly disappears at $\alpha = 0$.

3.2. Estimating the normal disc velocities

The local divergence from BEM in sheared inflow may influence the results of simple design codes, as most of them use BEM-based models to determine the normal velocities at the rotor. Madsen *et al.* [14] compared different BEM implementations with full rotor and AL simulations and found pronounced differences in the induced velocities even between the BEM implementations. They connected these differences to the exact procedure with which the induced velocities are estimated.

Following BEM theory the velocity at the disc is given by

$$u(\mathbf{x}) = [1 - a(\mathbf{x})]\, V_{\mathrm{ref}}(\mathbf{x}) \quad \text{with} \quad a(\mathbf{x}) = f(C_t(\mathbf{x})) \tag{2}$$

,where the induction is itself a function of the thrust coefficient. Here the fit by Madsen [15] is used to relate C_t with a (also see figure 4). Equation (2) leads to very different disc velocities depending on the choices for $C_t(\mathbf{x})$ and $V_{\mathrm{ref}}(\mathbf{x})$. Table 1 lists the different combinations tested in this analysis. The first 6 methods set the local thrust to the global thrust coefficient ($C_t(\mathbf{x}) = C_T$), but the definition of the reference velocity for computing the coefficient varies. The same reference velocity is used for determining the disc velocities. Methods #7-12 follow the same approach as previous once with regard to C_T, but use the actual inflow profile $V_\infty(\mathbf{x})$ to arrive at the disc velocities. The last three methods #13-15 use more local definitions of the thrust coefficient.

Table 1. Different definitions for estimating the induced velocities following equation (2). Here $c = {}^1\!/\!_2\rho$ and the average is abbreviated with $\langle a \rangle_b = \int_b a\,\mathrm{d}b / \int_b \mathrm{d}b$.

#	$C_t(\mathbf{x})$	$V_{\mathrm{ref}}(\mathbf{x})$
1	$C_T = \left(\int_A f_N(\mathbf{x})\,\mathrm{d}A\right)\left(cV^2_{\{\infty,\mathrm{hub}\}}A\right)^{-1}$	$V_{\{\infty,\mathrm{hub}\}}$
2	$C_T = \left(\int_A f_N(\mathbf{x})\,\mathrm{d}A\right)\left(c\langle V_\infty(\mathbf{x})\rangle^2_A A\right)^{-1}$	$\langle V_\infty(\mathbf{x})\rangle_A$
3	$C_T = \left(\int_A f_N(\mathbf{x})\,\mathrm{d}A\right)\left(c\langle V^2_\infty(\mathbf{x})\rangle_A A\right)^{-1}$	$\sqrt{\langle V^2_\infty(\mathbf{x})\rangle_A}$
4	$C_T = \left(\int_A C_t(r)\,\mathrm{d}A\right)A^{-1} \quad C_t(r) = \left(\int_\theta f_N(\mathbf{x})\,\mathrm{d}\theta\right)\left(c\langle V_\infty(\mathbf{x})\rangle^2_\theta 2\pi r\right)^{-1}$	$\langle V_\infty(\mathbf{x})\rangle_\theta$
5	$C_T = \left(\int_A C_t(r)\,\mathrm{d}A\right)A^{-1} \quad C_t(r) = \left(\int_\theta f_N(\mathbf{x})\,\mathrm{d}\theta\right)\left(c\langle V^2_\infty(\mathbf{x})\rangle_\theta 2\pi r\right)^{-1}$	$\sqrt{\langle V^2_\infty(\mathbf{x})\rangle_\theta}$
6	$C_T = \left(\int_A C_t(\mathbf{x})\,\mathrm{d}A\right)A^{-1} \quad C_t(\mathbf{x}) = \left(f_N(\mathbf{x})\right)\left(cV^2_\infty(\mathbf{x})\right)^{-1}$	$\sqrt{\langle V^2_\infty(\mathbf{x})\rangle_A}$
7	Equivalent to # 1	$V_\infty(\mathbf{x})$
8	Equivalent to # 2	$V_\infty(\mathbf{x})$
9	Equivalent to # 3	$V_\infty(\mathbf{x})$
10	Equivalent to # 4	$V_\infty(\mathbf{x})$
11	Equivalent to # 5	$V_\infty(\mathbf{x})$
12	Equivalent to # 6	$V_\infty(\mathbf{x})$
13	$C_t(r) = \left(\int_\theta f_N(\mathbf{x})\,\mathrm{d}\theta\right)\left(c\langle V_\infty(\mathbf{x})\rangle^2_\theta 2\pi r\right)^{-1}$	$V_\infty(\mathbf{x})$
14	$C_t(r) = \left(\int_\theta f_N(\mathbf{x})\,\mathrm{d}\theta\right)\left(c\langle V^2_\infty(\mathbf{x})\rangle_\theta 2\pi r\right)^{-1}$	$V_\infty(\mathbf{x})$
15	$C_t(\mathbf{x}) = \left(f_N(\mathbf{x})\right)\left(cV^2_\infty(\mathbf{x})\right)^{-1}$	$V_\infty(\mathbf{x})$

Figure 3 shows the variation of the global thrust coefficient for the first six methods with the shear parameter. Methods #2+4 and #3+5 are almost equivalent. The simulations where set-up such that the kinetic energy over the disc is constant ($\int_A V_\infty^2 \, \mathrm{d}A = \text{const}$) with changing shear. Therefore it is unsurprising that methods #3+5 - using the integrated disc kinetic energy for normalisation - show nearly no variation in C_T with shear. The slight drop in C_T basically derives from a drop in the total normal force on the rotor. Except for method #6, the global thrust coefficients are similar. All definitions presented in table 1 are substituted

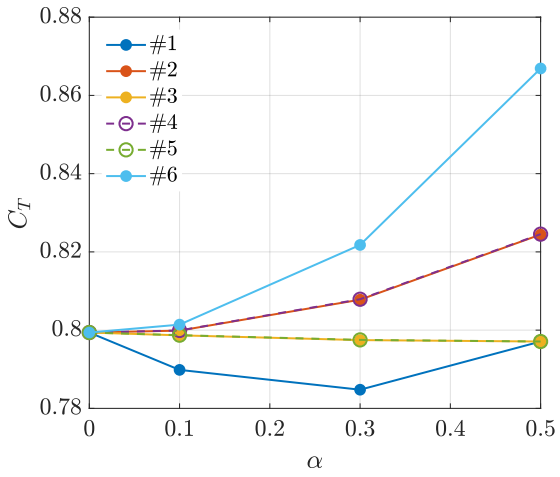

Figure 5. Global thrust coefficients computed with the methods described in table 1 as function of inflow shear parameter.

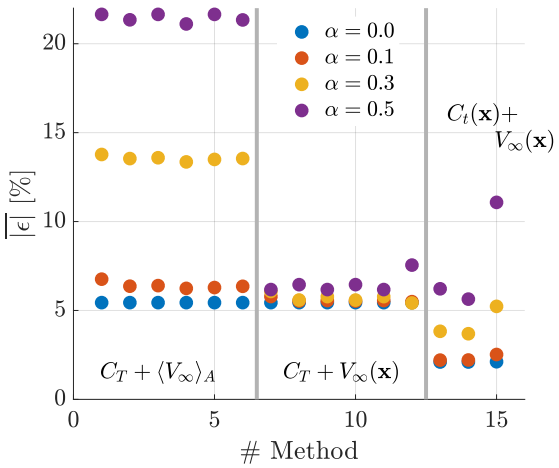

Figure 6. Mean absolute error in the estimated normal disc velocities following the methods in table 1 for changing shear.

into equation (2) to estimate the disc velocities using the forces $f_N((x))$ extracted from the LES simulations. They are subsequently compared to the actual velocities registered by the simulations. The error in the estimated disc velocities is thus given by

$$\epsilon(\mathbf{x}) = \frac{u(\mathbf{x}) - u_{\mathrm{LES}}(\mathbf{x})}{\sqrt{u_{\mathrm{LES}}^2 + v_{t,\mathrm{LES}}^2}} \tag{3}$$

where $\sqrt{u_{\mathrm{LES}}^2 + v_{t,\mathrm{LES}}^2}$ represents the velocity magnitude acting at the blade. The local absolute error is weighted by the corresponding area to derive error statistics like upper/lower quartiles and average error. Figure 6 depicts the mean absolute error - representative for the entire error distribution - for the different methods given in table 1 and changing shear. For moderate shear ($\alpha \leq 0.1$) all methods using the global thrust coefficient arrive at similar average errors. The methods with more local thrust definitions achieve 3% lower errors. Increasing shear rapidly increases the error for methods which do not use the local inflow velocity field $V_\infty(\mathbf{x})$. Generally, applying a more local definition of the thrust coefficient seems more beneficial, though it disappears in face of more extreme shear ($\alpha = 0.5$). Interestingly, an annularly averaged thrust coefficient as used in #13+14 outperforms the strictly local definition of #15. This is related to the previously mentioned pronounced correlation over the annuli of the disc, which is also visible in figures 1 and 2. The blade forces (not shown) react to the changes in the normal velocity - as they cause a change in the angle of attack - but this behaviour is not strictly local. This is also reflected in the extremely large local thrust coefficients observed at $\alpha = 0.5$ in figure 3. By taking annular averaged thrust coefficients the variation in C_t over the disc is greatly reduced -

covering a range of 20% relative to the mean, compared to 160% using a strictly local definition. In fact the BEM predicted connection between C_t and a (see figure 4) is recovered using the annular definition of the thrust coefficient.

3.3. Estimating velocities upstream of rotor

Whereas the disc velocities are important for predicting turbine loads, the upstream deceleration in front of a rotor is of interest in power performance evaluation [4] and predictive control [16].

Troldborg and Meyer Forsting [3] devised a semi-analytical model from AL simulations of multiple rotors, that uses a vortex sheet formulation along the axial direction and a shape function for the radial dimension:

$$\tilde{u}(\tilde{x},\tilde{r},C_T) = 1 - \overbrace{a(\tilde{x},C_T)}^{\text{axial}}\underbrace{f(\epsilon)}_{\text{radial}} \tag{4}$$

Here the $\tilde{\bullet}$ represents normalised quantities. For the detailed definitions refer to [3]. Numerically, Meyer Forsting *et al.* [1] showed the model to perform acceptably in moderate shear. Borraccino *et al.* [4] applied the model to lidar measurements taken upstream of a commercial multi-megawatt turbine and reported positively on its accuracy. In this section previous work is

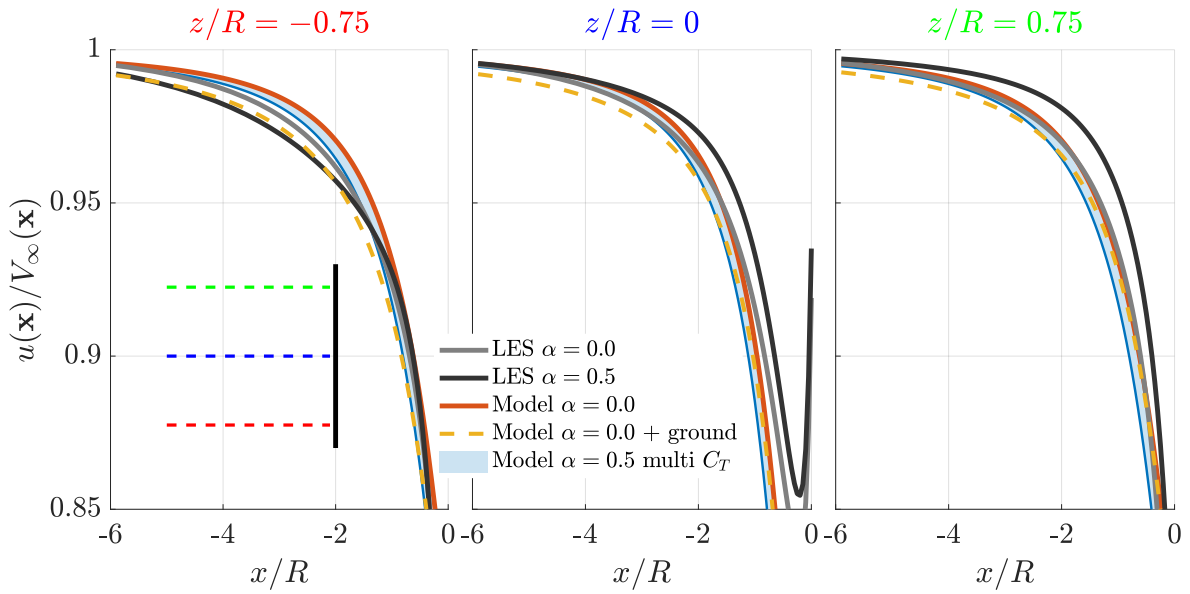

Figure 7. Normalised axial velocity upstream along three lines at different vertical positions of the rotor (see schematic in the lower left corner of the first frame) predicted by LES simulations and by the simple induction zone model in equation (4) for two different shear parameters. Note that the simple model does not account for shear, but the global thrust coefficient may change as shown in figure 5. The ground effect is modelled via a mirror turbine.

expanded to more strongly sheared inflow. Figure 7 compares the axial velocity upstream from the LES simulations with those predicted by the simple model along three vertical stations of the rotor (see lower left corner of first frame for a visual representation of the lines with respect to the rotor). As the latter only uses the global C_T, solely the values obtained from methods #1-6 are applied. Without shear ($\alpha = 0$) all methods yield the same coefficient, thus only a single line is shown for this case, whereas a shaded region is depicted for $\alpha = 0.5$ as the global thrust

varies depending on its definition (see figure 5). Note that only the thrust coefficients change in the simple model - it does not account for shear, but imposes the induced velocities on the inflow profile. Without shear the simple model agrees well with the LES results, only showing slight deviation closer to the ground. For strong shear the LES exhibits strong changes in the induced velocity with distance from the ground. At $z/R = -0.75$ there is stronger induction at large shear beyond $1R$ upstream. This picture is reversed moving upwards, as the velocity deficit is reduced compared to no shear. Lower induction indicates lower loading in this region, which is supported by the local thrust field shown in figure 3. Applying a more local definition of thrust in the simple model could therefore also be beneficial.

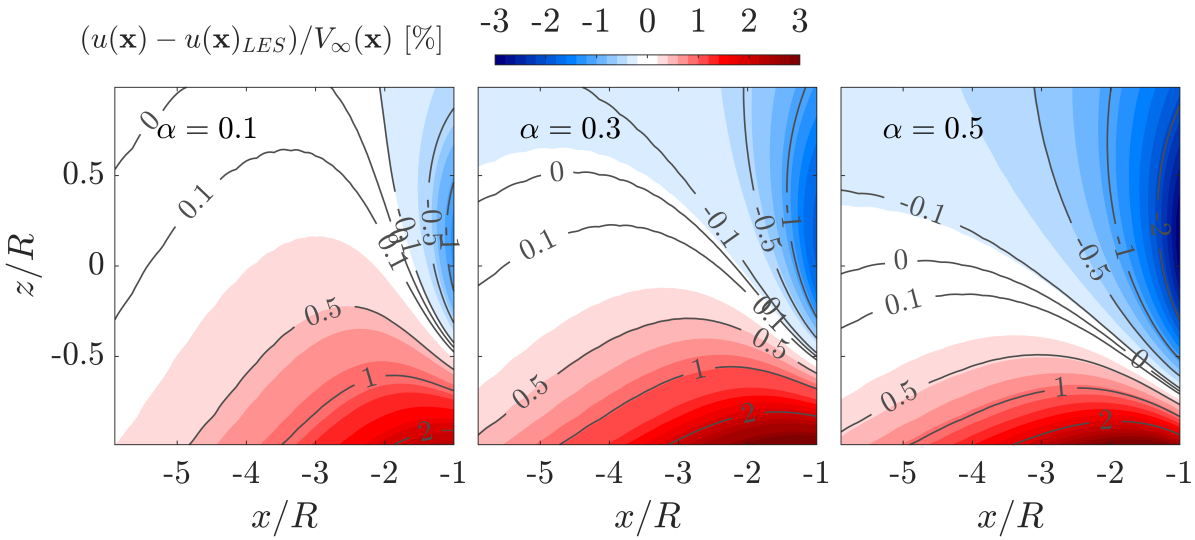

Figure 8. Error in the estimated velocities upstream of the rotor for varying shear in the xz-plane (crossing rotor plane) at $y/R = 0$. The rotor centre lies at $(0, 0, 0)$.

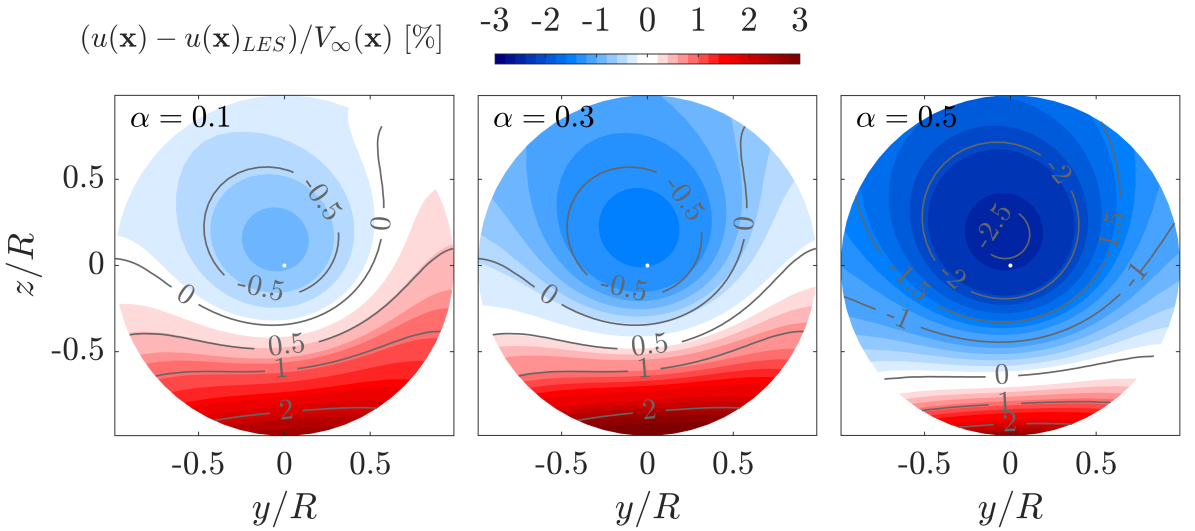

Figure 9. Error in the estimated velocities in planes parallel to the rotor disc at $x/R = -1$ upstream for varying shear. The rotor centre lies at $(0, 0, 0)$.

As suggested by Branlard [17] and Meyer Forsting [1] an image vortex system is implemented to represent the ground - this equivalent to superposing the induced velocities of a neighbouring turbine located two hub heights downwards. Unfortunately, this does not improve the predictions, except close to the ground.

Figures 8 and 9 give a more complete overview of the simple model error and its evolution with shear. The former shows the errors in the xz-plane through $y/R = 0$ (along the rotor centreline) and the latter in the yz-plane parallel to the disc at $x/R = -1$. The error increases with shear, but is limited to $\pm 0.5\%$ of the local free-stream velocity in the region $z/R > -0.25$ and $x/R < -3$. The yz-planes clearly show the asymmetry of the induction and depict the over-prediction of the normal velocity close to the ground. The under-prediction is circular above hub height and the zero error line moves downwards with increasing shear.

4. Conclusion

LES simulations with an actuator line representation of the rotor confirm the linearity assumption for moderate wind shear. To estimate the normal velocities at the disc the annularly averaged thrust coefficient is best suited when the induction is imposed on the inflow profile. A strictly local definition of the thrust and induction leads to strong over-prediction of the induction in the rotor plane near the ground. Forces and induction exhibit a strong annular correlation over the rotor, such that the inflow velocity profile cannot simply be mapped onto the rotor. A simple induction zone model devised for uniform inflow estimates the velocity upstream within $\pm 0.5\%$ even in extreme shear over a region which covers the upper half of the rotor and is at least three rotor radii away from the turbine. The addition of a mirror vortex system - modelling the ground effect - does not improve the results, as it leads to over-prediction of the induction.

Acknowledgments

This work was performed inside the UniTTe project (unitte.dk), which is partially financed by The Innovation Fund Denmark, grant number 1305-00024B.

References

[1] Meyer Forsting A, Troldborg N, Bechmann A and Réthoré P E 2017 *Modelling Wind Turbine Inflow: The Induction Zone* Ph.D. thesis DTU Wind Energy Denmark
[2] Simley E, Angelou N, Mikkelsen T, Sjöholm M, Mann J and Pao L Y 2016 *Journal of Renewable and Sustainable Energy* **8**
[3] Troldborg N and Meyer Forsting A R 2017 *Wind Energy* ISSN 1099-1824 we.2137 URL `http://dx.doi.org/10.1002/we.2137`
[4] Borraccino A, Schlipf D, Haizmann F and Wagner R 2017 *Wind Energy Science Discussions* **2** 269–283 ISSN 2366-7621
[5] Sørensen N 1995 *General purpose flow solver applied to flow over hills* Ph.D. thesis Risø National Laboratory
[6] Menter F R 1993 Zonal two equation $k-\omega$ turbulence models for aerodynamic flows 23^{rd} *Fluid Dynamics, Plasmadynamics, and Lasers Conference, Fluid Dynamics and Co-located Conferences* (Orlando,FL)
[7] Phouc T 1994 *Modèles de sous maille appliqués aux écoulmements instationnaires décollés* (LIMSI)
[8] Strelets M 2001 Detached eddy simulation of massively separated flows 39^{th} *AIAA Aerospace Sciences Meeting and Exhibit* AIAA Paper 2001-0879 (Reno,NV)
[9] Leonard B 1979 *Computer Methods in Applied Mechanics and Engineering* **19** 59–98
[10] Jonkerman J, Butterfield S, Musial W and Scott G 2009 Definition of a 5-mw reference wind turbine for offshore system development Tech. rep. NREL
[11] Srensen J N and Shen W Z 2002 *Journal of Fluids Engineering* **124** 393–399
[12] Troldborg N, Sørensen J and Mikkelsen R 2009 *Actuator Line Modeling of Wind Turbine Wakes* Ph.D. thesis Technical University of Denmark
[13] Shen W, Srensen J and Mikkelsen R 2004 *Tip loss correction for actuator / Navier Stokes computations* (Delft University of Technology) pp 138–144

[14] Madsen H A, Riziotis V, Zahle F, Hansen M, Snel H, Grasso F, Larsen T, Politis E and Rasmussen F 2012 *Wind Energy* **15** 63–81 ISSN 1099-1824 URL `http://dx.doi.org/10.1002/we.493`

[15] Aagaard Madsen H 1997 *A CFD analysis of the actuator disc flow compared with momentum theory results* (Technical University of Denmark. Department of Fluid Mechanics) pp 109–124

[16] Schlipf D, Fleming P, Haizmann F, Scholbrock A K, Hofsäß M, Wrigth A and Cheng P W 2012 Field testing of feedforward collective pitch control on the cart2 using a nacelle-based lidar scanner *The Science of Making Torque from Wind*

[17] Branlard E 2017 *Wind Turbine Aerodynamics and Vorticity-Based Methods* (*Research Topics in Wind Energy* vol 7) (Springer)